AGU ADVANCING EARTH AND SPACE SCIENCE

Geophysical Research Letters®

RESEARCH LETTER
10.1029/2021GL095878

Special Section:
The COVID-19 pandemic: linking health, society and environment

The Seesaw Pattern of $PM_{2.5}$ Interannual Anomalies Between Beijing-Tianjin-Hebei and Yangtze River Delta Across Eastern China in Winter

Xiaohui Liu[1], Bin Zhu[1], Tong Zhu[2], and Hong Liao[3]

[1]Collaborative Innovation Center on Forecast and Evaluation of Meteorological Disasters and Key Laboratory of Meteorological Disaster, Ministry of Education (KLME), Nanjing University of Information Science & Technology, Nanjing, China, [2]IMSG at NOAA/NESDIS/STAR, College Park, MD, USA, [3]Jiangsu Key Laboratory of Atmospheric Environment Monitoring and Pollution Control, Collaborative Innovation Center of Atmospheric Environment and Equipment Technology, School of Environmental Science and Engineering, Nanjing University of Information Science & Technology, Nanjing, China

Key Points:

- A seesaw pattern of $PM_{2.5}$ interannual anomalies between Beijing-Tianjin-Hebei (BTH) and Yangtze River Delta was found
- The difference in regional transport driven by interannual variation of the East Asian winter monsoon (EAWM) was the dominant mechanism
- Higher $PM_{2.5}$ anomalies in northern BTH during the COVID-19 lockdown were mainly caused by the nonactive EAWM

Supporting Information:

Supporting Information may be found in the online version of this article.

Correspondence to:

B. Zhu,
binzhu@nuist.edu.cn

Citation:

Liu, X., Zhu, B., Zhu, T., & Liao, H. (2022). The seesaw pattern of $PM_{2.5}$ interannual anomalies between Beijing-Tianjin-Hebei and Yangtze River Delta across eastern China in winter. *Geophysical Research Letters*, *49*, e2021GL095878. https://doi.org/10.1029/2021GL095878

Received 2 SEP 2021
Accepted 20 DEC 2021

Author Contributions:

Conceptualization: Bin Zhu
Methodology: Xiaohui Liu
Project Administration: Hong Liao
Supervision: Bin Zhu, Tong Zhu
Writing – original draft: Xiaohui Liu
Writing – review & editing: Xiaohui Liu, Bin Zhu, Tong Zhu

Abstract Since 2013, the winter mean fine particulate matter ($PM_{2.5}$) had been decreased significantly due to stringent emission controls in most of China. Nevertheless, we found a seesaw pattern of $PM_{2.5}$ interannual anomalies between Beijing-Tianjin-Hebei (BTH) and Yangtze River Delta (YRD). Using the multiple linear regression method, meteorology-driven $PM_{2.5}$ interannual anomalies show that the low (high) $PM_{2.5}$ relative difference between BTH and YRD ($RD_{B\&Y}$) was associated with the strong (weak) East Asian winter monsoon (EAWM). The strong EAWM transported more air pollutants from BTH to YRD. During the COVID-19 lockdown period, due to the weak EAWM, air pollution still occurred in northern BTH, while the $PM_{2.5}$ was relatively low in YRD, causing high $RD_{B\&Y}$ values. Our results imply that the activity of EAWM and characteristics of regional transport have obvious interannual variations, which is indispensable in evaluating the achievements of $PM_{2.5}$ quality management between up and downstream regions.

Plain Language Summary In winter, periodic changes of particulate matter ($PM_{2.5}$) over eastern China are governed by recurrent meteorological conditions, for example, cold front outbreaks and stagnant weather. In Beijing-Tianjin-Hebei (BTH), stagnant weather is more likely to cause air pollution, while cold air has an obvious effect on removing $PM_{2.5}$. Conversely, air pollutants transported by cold air from BTH to Yangtze River Delta (YRD) frequently occurred. Since 2013, the annual average $PM_{2.5}$ concentration in eastern China has been reduced due to strict emission controls. In this study, we found a seesaw pattern of $PM_{2.5}$ interannual anomalies between BTH and YRD related to the activity of East Asian winter monsoon (EAWM). In the active EAWM years, the $PM_{2.5}$ relative difference between BTH and YRD ($RD_{B\&Y}$) was slight because the meteorological factors favored $PM_{2.5}$ diffusion in BTH and high $PM_{2.5}$ transport from BTH to YRD. In the weak EAWM years, for example, during the COVID-19 lockdown period, meteorological factors did not favor $PM_{2.5}$ diffusion over BTH and high $PM_{2.5}$ transport from BTH to YRD, leading to a large $RD_{B\&Y}$. The results show that interannual variation of EAWM and regional transport are crucial indicators for evaluating the effect of air quality control and management between up and down regions.

1. Introduction

Since the "Air Pollution Prevention and Control Action Plan" was implemented in 2013, strictly controlled emissions resulted in obvious reductions in the annual average particulate matter ($PM_{2.5}$) concentration across most of China (Zheng et al., 2018). However, many regions in China still experience heavy air pollution in winter, such as in Beijing-Tianjin-Hebei (BTH) and Yangtze River Delta (YRD) (Hou et al., 2020; J. Li et al., 2017). For example, during the lockdown period (February 2020) caused by Coronavirus Disease 2019 ($COVID\text{-}19_{lock\text{-}periods}$), anthropogenic emissions were greatly constrained, while air pollution still occurred over BTH (Z. L. Wang et al., 2021).

The frequent heavy air pollution events in winter are mainly attributed to unfavorable meteorological conditions and relatively high anthropogenic emissions (Xu et al., 2011). Meteorological factors, such as wind speed, planetary boundary layer height (PBLH), and relative humidity, play crucial roles in the transport, dispersion, chemical transformation, and deposition of air pollutants (Z. Q. Li et al., 2017; Liu et al., 2020). In winter, cold fronts periodically break out and move through northern to southern China (Guo et al., 2014), transporting air

pollutants quickly and effectively to downstream regions, such as YRD (Huang et al., 2020; Kang et al., 2019). Many previous studies have mainly focused on the effects of meteorological conditions and $PM_{2.5}$ emissions on regional pollution (Z. Chen et al., 2018; Yang et al., 2021). However, few studies have quantitatively described the relations of $PM_{2.5}$ between up- and downstream regions in interannual variations.

In this study, we used a stepwise multiple linear regression (MLR) method to quantitatively fit the $PM_{2.5}$ interannual variation driven by meteorology between BTH and YRD. Furthermore, we addressed the effect of EAWM on the interannual relative differences in $PM_{2.5}$ between the two regions, including the $COVID\text{-}19_{lock\text{-}periods}$.

2. Data and Methods

2.1. Observations Data

We used hourly $PM_{2.5}$ data during winter 2013–2019 from the National Urban Air Quality Real-time Publishing Platform. The data set had nearly 1,500 ambient air quality monitoring stations, including 330 cities, and covered most of China. In this study, we focused on two polluted regions, BTH (36°N–43°N, 114°E–120°E) and YRD (29.5°N–33.5°N, 118°E–122.5°E), in East China. BTH and YRD had 13 cities (Figure S1 in Supporting Information S1), and their corresponding air quality monitoring stations were 66 and 71, respectively. The $PM_{2.5}$ concentrations were measured using the β-absorption method or the micro-oscillating balance method (MEE, 2012). Quality control of the hourly data was performed according to Hou et al. (2020). The average $PM_{2.5}$ concentrations over BTH and YRD were obtained from the cities (Figure S1 in Supporting Information S1) in the regions. The 500-hPa geopotential height (H_{500}), 850-hPa meridional wind velocity (V_{850}), 1000-hPa relative humidity (RH_{1000}) were obtained from ECMWF Reanalysis v5 (ERA-5) hourly data on pressure levels ($1° \times 1°$), and PBLH was obtained from the ERA-5 hourly data on single levels ($1° \times 1°$) in winter (December-January-February) during 2013–2019. The data quality of variables in ERA-5 over eastern China is discussed in Text S1 in Supporting Information S1.

2.2. Quantification of Meteorological Contributions

In this study, based on our previous analysis of the correlation between $PM_{2.5}$ and 26 meteorological factors (Liu et al., 2020), we chose the most significant factors with regional correlation coefficients passing the 0.05 significance test as the dominant meteorological factors. They are H_{500}, V_{850}, RH_{1000}, and PBLH, which influence $PM_{2.5}$ will be discussed in Section 3.2. Based on the hourly data of $PM_{2.5}$ and the dominant meteorological factors, by removing the 50-day moving average values from the synoptic-scale values (10-day mean), we obtained the detrended data set of $PM_{2.5}$ and the dominant meteorological factors following the method in Zhai et al. (2019). The detrended data set focuses on the synoptic-scale of variability and eliminates the long-term trends (Shen et al., 2017; Tai et al., 2010). The 10-day mean synoptic-scale values were selected by comparing the correlations between the dominant meteorological factors and $PM_{2.5}$ at different time-averaging scales (3-day, 6-day, 10-day, and 15-day) (Figure S5 in Supporting Information S1). The correlations of the 10-day time scale were more significant than the others in both BTH and YRD (Text S2 in Supporting Information S1), which could reasonably reflect the relationship between synoptic-scale meteorological factors and $PM_{2.5}$ variations.

Using the detrended data set, we first fitted $PM_{2.5}$ with meteorological factors at each city over BTH and YRD. The formula was as follows:

$$Y_i(t) = \sum_{n=1}^{4} \alpha_{i,n} X_{i,n}(t) + b_i \quad (1)$$

where $Y_i(t)$ is the detrended $PM_{2.5}$ for each city (i), and $X_{i,n}(t)$ is the corresponding detrended dominant meteorological factor $n\epsilon[1,4]$. The $\alpha_{i,n}$ and b_i are the regression coefficients and intercepts, respectively.

Second, we use the MLR method as in Zhai et al. (2019) to quantify the effect of meteorological on $PM_{2.5}$. The meteorological anomalies in winters of 2013–2019 were obtained by removing the 7-year means of the 50-day moving averages from the 10-day averaged time series. Then, applying this result to the formula 1, the meteorology-driven $PM_{2.5}$ anomalies were obtained. Similar MLR methods have been successfully applied to quantify the meteorological effect on other air pollutants (K. Li et al., 2019; Otero et al., 2018).

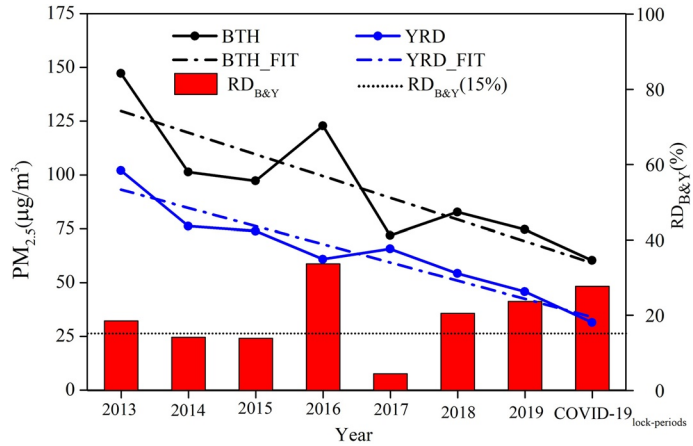

Figure 1. The mean $PM_{2.5}$ concentrations in winters of 2013–2019 and during the $COVID\text{-}19_{lock\text{-}periods}$; the observed concentration of $PM_{2.5}$ (solid lines) and the linear regression trends (dotted lines) in BTH (black) and YRD (blue) regions. The bar shows the $RD_{B\&Y}$, with the dotted line being 15%.

3. Results and Discussion

3.1. $PM_{2.5}$ Trends in BTH and YRD, 2013–2019

Figure 1 shows the trends of average $PM_{2.5}$ decrease in both BTH and YRD mostly because of the effective emission reductions since 2013. We found inconsistent interannual $PM_{2.5}$ variations in the two regions in some years. For example, $PM_{2.5}$ increased considerably in 2016 but decreased much in 2017 in BTH. In contrast, the $PM_{2.5}$ decreased in 2016 but increased in 2017 in YRD. We defined the $PM_{2.5}$ relative difference between BTH and YRD ($RD_{B\&Y}$) by calculating the ratio of the difference in the $PM_{2.5}$ concentration in the two regions to the sum of the $PM_{2.5}$ concentration in the two regions: $(BTH_{PM2.5} - YRD_{PM2.5})/(BTH_{PM2.5} + YRD_{PM2.5})$. The calculated $RD_{B\&Y}$ was higher (>15%) in 2013, 2016, 2018, and 2019, but lower (<15%) in 2014, 2015, and 2017. The $RD_{B\&Y}$ was highest in 2016 (33.7%) and lowest in 2017 (4.5%).

After removing the decreasing trend of emission in this period, we found an obvious seesaw pattern of the $PM_{2.5}$ anomalies between BTH and YRD cities in 2016 and 2017 (Figure 2), and the other years are shown in Figure S8 in Supporting Information S1. In winter of 2016 (Figure 2a), the detrended $PM_{2.5}$ anomalies were positive in BTH but negative in YRD. Oppositely, in 2017 (Figure 2b), the detrended $PM_{2.5}$ anomalies were negative in BTH but positive in YRD. During the $COVID\text{-}19_{lock\text{-}periods}$ (Figure 2c), although obvious emission reductions occurred in

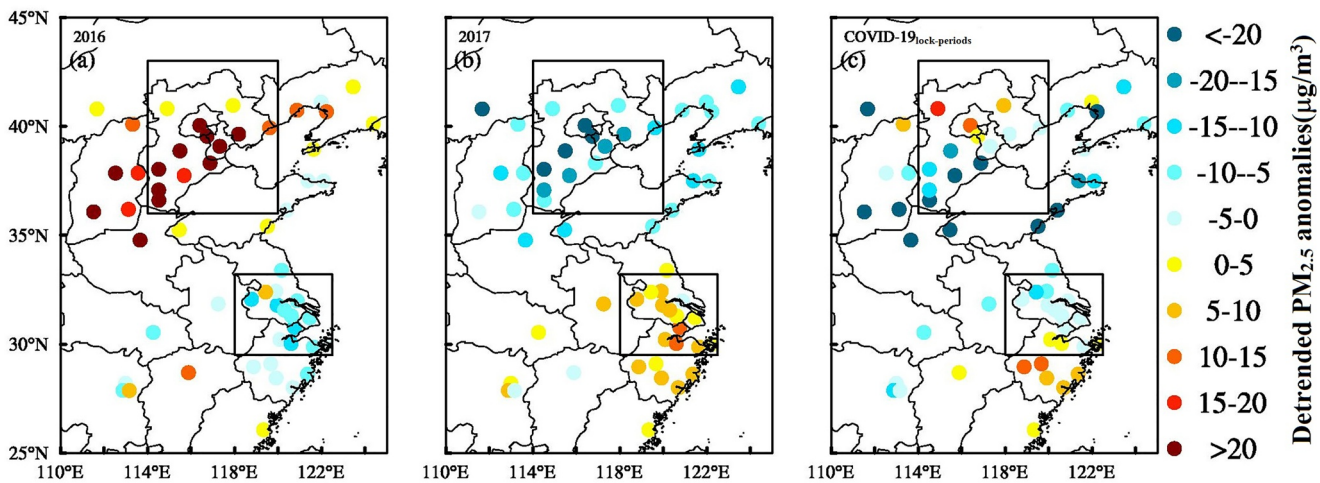

Figure 2. The detrended $PM_{2.5}$ anomalies in winters of 2016, 2017, and the $COVID\text{-}19_{lock\text{-}periods}$ for each city in East China (a) 2016, (b) 2017, and (c) $COVID\text{-}19_{lock\text{-}periods}$.

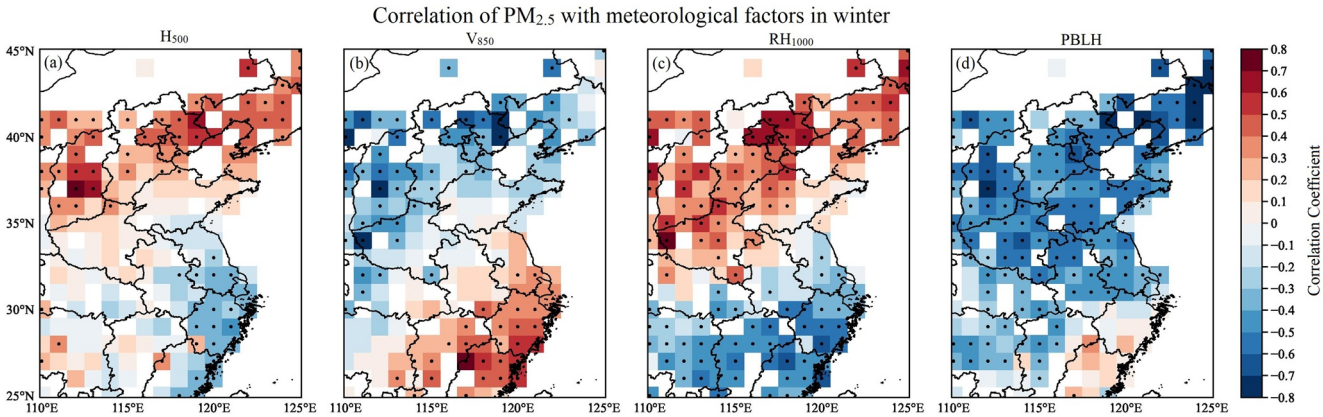

Figure 3. The correlation coefficients on the 1° × 1° grid of the 10-day average $PM_{2.5}$ with four individual meteorological factors in winters of 2013–2019 over eastern China. (a) H_{500}, (b) V_{850}, (c) RH_{1000}, and (d) PBLH. Dots indicate statistically significant correlations ($p < 0.05$).

both BTH and YRD, significant positive detrended $PM_{2.5}$ anomalies were found in northern BTH, and negative detrended $PM_{2.5}$ anomalies were found in YRD, resulting in the second-highest $RD_{B\&Y}$ value of 27.7%, as shown in Figure 1.

Because the measured emission reductions have been similar in BTH and YRD since 2013 (Q. Zhang et al., 2019), the cause of the seesaw pattern of the $PM_{2.5}$ anomalies in the two regions and the interannual variation in $RD_{B\&Y}$ may be attributed mainly to the synoptic-scale meteorological variations.

3.2. Dominant Meteorological Factors Related to $PM_{2.5}$

In wintertime, the most dominant weather system over East China is EAWM, and the interannual variation of EAWM is mainly characterized by meridional wind anomalies. Besides, the upstream atmospheric wave trains and the El Niño-Southern Oscillation-related Sea surface temperature anomalies also contribute to the generation of the meridional wind anomalies over East China (S. F. Chen et al., 2019). The alteration of cyclone and anticyclone on synoptic-scale causes periodic changes in $PM_{2.5}$ (Guo et al., 2014) in wintertime over East Asia.

Using the method described in Section 2.2, we obtained the dominant meteorological factors (H_{500}, V_{850}, RH_{1000}, and PBLH) that affected $PM_{2.5}$ over BTH and YRD on the synoptic-scale. Note here V_{850} is referred to the northerly wind (positive sign), which is commonly used to define the EAWM index. Figure 3 shows that the grid correlations of H_{500}, V_{850}, and RH_{1000} with $PM_{2.5}$ were positive over BTH but negative over YRD. The opposite correlations of $PM_{2.5}$ and H_{500} over BTH and YRD may be related to the large-scale vertical movement below H_{500}. As shown in Figure S6 in Supporting Information S1, in 2016, 2018, and 2019 (vs. 2014, 2015, and 2017), the upward (downward) draft anomaly occurred below 500 hPa in BTH and YRD. X. Y. Zhang et al. (2021) also found the opposite effect of vertical movement below 500 hPa on $PM_{2.5}$ in BTH and YRD. For example, in 2016, 2018, 2019, and $COVID\text{-}19_{lock\text{-}periods}$, with H_{500} positive anomalies, southerly and updraft anomalies below 500 hPa, air pollutants accumulated due to blocking and weak convergence in front of mountains, and the terrain forced the airflow to rise, resulting in an increase in humidity; these conditions were favorable for the occurrence of pollution events in BTH. However, due to the flat terrain in YRD, upward drafts are beneficial to the diffusion of pollution.

Generally, the averaged V_{850} in winter represents the activity of EAWM (J. P. Li & Zeng, 2002). A larger V_{850} is favorable for the diffusion of air pollutants to downstream over BTH (Cai et al., 2017). However, over YRD, the strong northerly wind (V_{850}) reflects that more air pollutants would be transported from BTH to YRD. Therefore, the active EAWM is beneficial to the lower $PM_{2.5}$ over BTH and the higher $PM_{2.5}$ over YRD.

The positive correlation between $PM_{2.5}$ and RH_{1000} is partly attributed to the role of heterogeneous and aqueous-phase aerosol chemistry in driving secondary $PM_{2.5}$ formation over BTH (Huang et al., 2020; Tie et al., 2017). Differently, over YRD, the high relative humidity may be related to precipitation, which is beneficial to $PM_{2.5}$ wet removal (Leung et al., 2018). The PBLH was negatively correlated with $PM_{2.5}$ in most parts of China, while

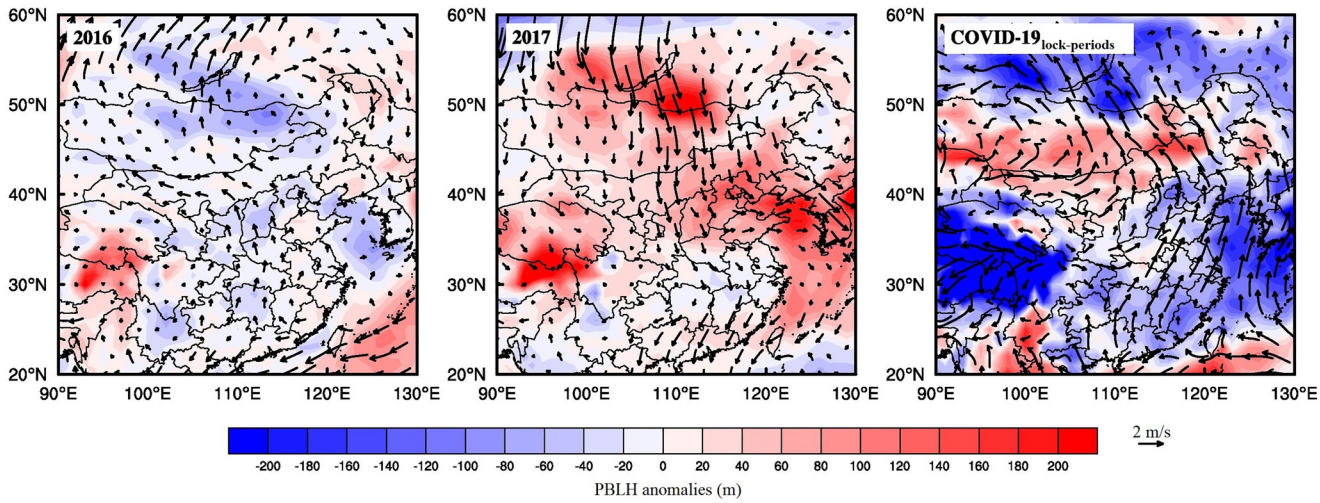

Figure 4. Anomalies of 850-hPa wind and PBLH in 2016, 2017, and COVID-$19_{\text{lock-periods}}$ over eastern China. The vectors indicate the 850-hPa wind field, and the shading represents the PBLH. The anomalies of 2016 and 2017 were obtained by removing the 7-year winter means from the winters of 2016 and 2017. For COVID-$19_{\text{lock-periods}}$, the anomaly was obtained by removing the 7-year means of February from the February 2020.

slightly positively correlated over southeast China, which was consistent with the results of previous studies (Lou et al., 2019; W. C. Zhang et al., 2018).

3.3. Meteorological Drivers of $PM_{2.5}$ Spatial Pattern

3.3.1. Meridional Wind Anomaly and Activity of EAWM

The four meteorological factors (H_{500}, V_{850}, RH_{1000}, and PBLH) reflect different aspects of EAWM. Both H_{500} and V_{850} can be used to study the activity of EAWM (H. J. Wang & Jiang, 2004; L. Wang et al., 2009). Figure 3 shows that the grid correlation of V_{850} and $PM_{2.5}$ is more obvious than that of H_{500} in BTH and YRD. Therefore, in Figure 4, we analyzed the anomalies of 850-hPa wind and PBLH in 2016, 2017, and COVID-$19_{\text{lock-periods}}$ (the other years are shown in Figure S7 in Supporting Information S1). The negative anomalies of V_{850} in 2016 and extremely negative anomalies in the COVID-$19_{\text{lock-periods}}$ indicated the nonactive EAWM and enhanced southeasterly over eastern China, which were not conducive to the transport of air pollutants from BTH to YRD. In addition, the negative PBLH anomaly in BTH was not conducive to the vertical diffusion of air pollutants. As such, the $RD_{B\&Y}$ was large in 2016 and the COVID-$19_{\text{lock-periods}}$.

In contrast, the positive V_{850} and PBLH anomalies in 2017 indicated an active EAWM and enhanced northerlies over eastern China, which were conducive to the transport of air pollutants from BTH to YRD by cold fronts, resulting in a low $RD_{B\&Y}$ in 2017. Therefore, the variation of EAWM activity can lead to significant differences in the low-level wind field and then affect the $RD_{B\&Y}$. Similar results could be obtained in other years (Figure S7 in Supporting Information S1).

We used the winter monsoon index (I_{Wang}) proposed by H. J. Wang and Jiang (2004), which is the average of the V_{850} anomalies covering the region of 110°E–122°E and 29°N–50°N to reflect the variations in EAWM. The years with positive and negative I_{Wang} values were defined as active winter monsoon years (Act) and nonactive winter monsoon years (Non-act). Table 1 shows that the I_{Wang} values were positive in 2014, 2015, and 2017 and negative in other years (including the COVID-$19_{\text{lock-periods}}$). We found that the $RD_{B\&Y}$ values were small in the Act years, but they were large in the Non-act years, which was consistent with Figure 2. For instance, in 2017, the active year of EAWM had the smallest $RD_{B\&Y}$ (4.5%). In contrast, in the COVID-$19_{\text{lock-periods}}$, due to the weaker EAWM, the largest $RD_{B\&Y}$ (27.7%) was observed. The correlation coefficient between I_{Wang} and $RD_{B\&Y}$ was −0.75 ($a = 0.02$), indicating that the activity of EAWM was closely related to $RD_{B\&Y}$.

Table 1
The I_{Wang}, $RD_{B\&Y}$, and Act/Non-Act Years of the EAWM From 2013 to 2019 and the COVID-$19_{Lock\text{-}Periods}$

Year	2013	2014	2015	2016	2017	2018	2019	COVID-$19_{lock\text{-}periods}$
I_{Wang}	−0.7	0.4	0.7	−0.3	0.9	−0.3	−1.1	−1.0
$RD_{B\&Y}$ (%)	18.5	14.2	13.9	33.7	4.5	20.5	23.7	27.7
Act/Non-act	Non-act	Act	Act	Non-act	Act	Non-act	Non-act	Non-act

3.3.2. Spatial Patterns of $PM_{2.5}$ Represented by Dominant Meteorological Factors

Finally, the meteorology-driven $PM_{2.5}$ for each city, using formula 1, was shown in Figure 5. In generally, the spatial patterns of the $PM_{2.5}$ positive and negative anomalies represented by meteorology-driven $PM_{2.5}$ were very similar to that of the observational detrended $PM_{2.5}$ anomalies (Figure 2 and Figure S8 in Supporting Information S1). In the Act years (2014, 2015, and 2017), the meteorology-driven $PM_{2.5}$ anomalies were negative over BTH but positive over YRD. For example, in 2017, meteorology-driven $PM_{2.5}$ negative anomalies were highest in BTH (−15.6 μg/m^3) and $PM_{2.5}$ positive anomalies highest in YRD (6.1 μg/m^3). This result indicates that the seesaw pattern of the $PM_{2.5}$ anomalies between BTH and YRD was mainly induced by interannual variations in EAWM.

In the Non-act years (2013, 2016, 2018, and 2019), the effects of meteorological factors on $PM_{2.5}$ anomalies were positive in BTH, with values of 8.5, 9.7, 1.7, and 22.1 μg/m^3, respectively, and negative in 2016 (−2.9 μg/m^3) and 2018 (−2.4 μg/m^3) in YRD, as expected. However, in YRD, the meteorology-driven $PM_{2.5}$ anomalies had small positive values in 2013 (3.4 μg/m^3) and 2019 (0.1 μg/m^3), against our expectation. In 2013, the vertical motion anomaly was not obvious below 500 hPa in YRD (Figure S6 in Supporting Information S1), reflecting the restrained vertical diffusion of local pollutants and causing a positive $PM_{2.5}$ anomaly. In 2019, the negative PBLH anomaly (Figure S6 in Supporting Information S1) caused a positive $PM_{2.5}$ anomaly.

During the COVID-$19_{lock\text{-}periods}$, human activities and anthropogenic emissions were greatly constrained. Nevertheless, high $PM_{2.5}$ concentrations were still observed in BTH (Z. L. Wang et al., 2021), and these high pollutions could be attributed to the meteorology-driven $PM_{2.5}$ positive anomaly in the northern BTH (17.3 μg/m^3). The

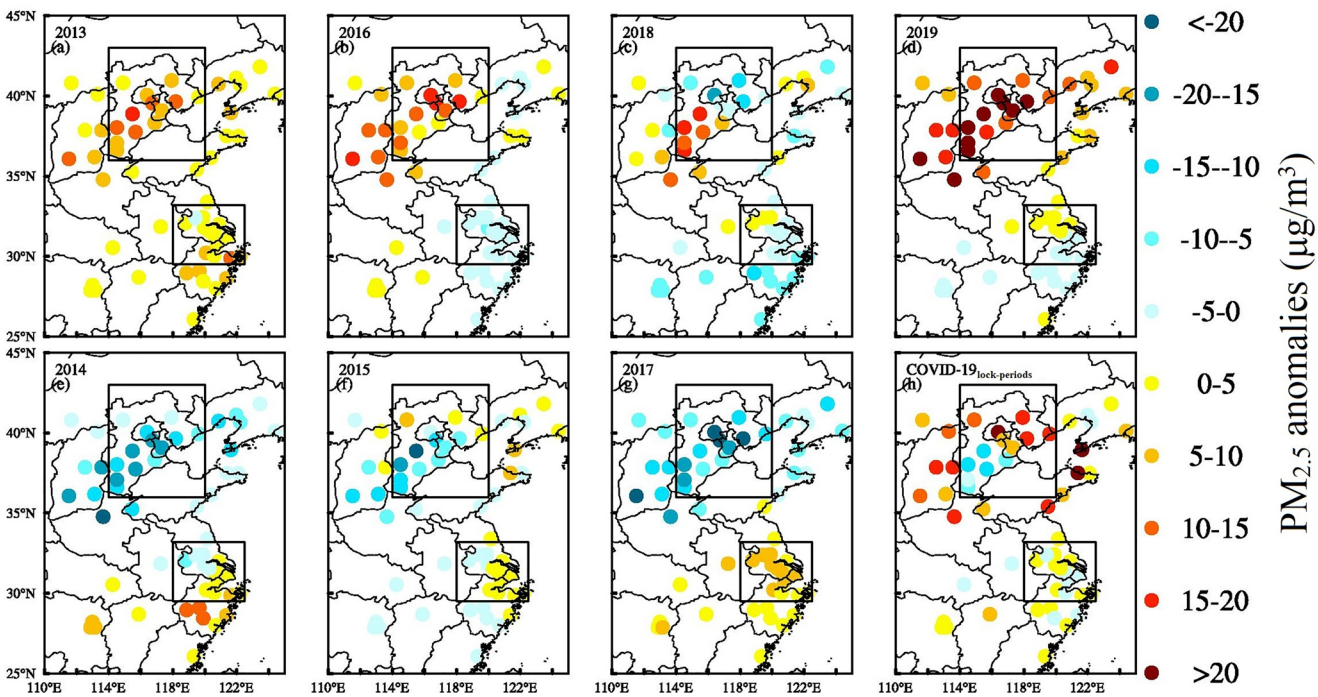

Figure 5. Meteorology-driven $PM_{2.5}$ anomalies of each city as determined from MLR in winters of 2013–2019 and COVID-$19_{lock\text{-}periods}$.

meteorology-driven $PM_{2.5}$ anomaly in northern BTH was more obvious than that in YRD (0.6 μg/m^3) and result in the large $RD_{B\&Y}$ (27.7%) during the COVID-19$_{lock\text{-}periods}$.

4. Conclusions

Since 2013, the annual average $PM_{2.5}$ concentration has been reduced considerably due to strict emission controls. However, a seesaw pattern of the $PM_{2.5}$ interannual anomalies between BTH and YRD was found in winters of 2013–2019 and during COVID-19$_{lock\text{-}periods}$. Using the MLR method, we revealed that the seesaw pattern was closely related to the activity of EAWM. In the Act years, there were smaller differences between the $PM_{2.5}$ concentrations over BTH and YRD regions, for example, in 2017, $RD_{B\&Y}$ = 4.5%, owing to the removal of $PM_{2.5}$ by cold air over BTH and the transport of high air pollutants from BTH to YRD. In the Non-act years, there were larger $PM_{2.5}$ differences between the two regions, for example, in 2016, $RD_{B\&Y}$ = 33.7%, and during the COVID-19$_{lock\text{-}periods}$ $RD_{B\&Y}$ = 27.7%.

We also derived meteorology-driven $PM_{2.5}$ anomalies by using the MLR method, which generally well captured the seesaw pattern of the interannual $PM_{2.5}$ anomalies. In the Act years (2014, 2015, and 2017), the meteorology-driven $PM_{2.5}$ anomalies were negative over BTH but positive over YRD, as expected. In the Non-act years (2013, 2016, 2018, and 2019), the meteorology-driven $PM_{2.5}$ anomalies were always positive over BTH and negative over YRD in 2016 and 2018. However, the small positive $PM_{2.5}$ anomalies in 2013 (3.4 μg/m^3) and 2019 (0.1 μg/m^3) were not as expected due to restrained vertical diffusion and depressed PBLH, respectively.

Notably, in the COVID-19$_{lock\text{-}periods}$, stagnant meteorological conditions were the main cause of pollution in the northern of BTH. The meteorology-driven positive $PM_{2.5}$ anomaly was more obvious in the northern of BTH (17.3 μg/m^3) than in YRD (0.6 μg/m^3). The large $RD_{B\&Y}$ was attributed to a weak EAWM.

Our results imply that the activity of EAWM and regional transport have obvious interannual variations and are indispensable in evaluating the achievements of $PM_{2.5}$ management in winter between upwind and downwind regions.

Data Availability Statement

The $PM_{2.5}$ observational data are obtained from the Ministry of Environmental Protection of China and the China Air Quality Online Monitoring and Analysis Platform (https://www.aqistudy.cn/) (only available in Chinese). The ERA-5 hourly data on pressure levels and on single levels are download from https://doi.org/10.24381/cds.bd0915c6 and https://doi.org/10.24381/cds.adbb2d47, respectively.

Acknowledgments
This work was supported by the National Natural Science Foundation of China (Grant Nos. 42021004 and 92044302) and the Postgraduate Research and Practice Innovation of Jiangsu Province Program (Grant No. SJKY19_0942).

References

Cai, W. J., Li, K., Liao, H., Wang, H. J., & Wu, L. X. (2017). Weather conditions conducive to Beijing severe haze more frequent under climate change. *Nature Climate Change*, *7*, 257–262. https://doi.org/10.1038/nclimate3249

Chen, S. F., Guo, J. P., Song, L. Y., Cohen, J. B., & Wang, Y. L. (2019). Temporal disparity of the atmospheric systems contributing to interannual variation of wintertime haze pollution in the North China Plain. *International Journal of Climatology*, *40*(1), 128–144. https://doi.org/10.1002/joc.6198

Chen, Z.Y, Xie, X., Cai, J., Chen, D., Gao, B., He, B., et al. (2018). Understanding meteorological influences on $PM_{2.5}$ concentrations across China: A temporal and spatial perspective. *Atmospheric Chemistry and Physics*, *18*(8), 5343–5358. https://doi.org/10.5194/acp-18-5343-2018

Guo, S., Hu, M., Zamora, M. L., Peng, J., Shang, D., Zheng, J., et al. (2014). Elucidating severe urban haze formation in China. *Proceedings of the National Academy of Sciences*, *111*(49), 17373–17378. https://doi.org/10.1073/pnas.1419604111

Hou, X. W., Zhu, B., Kumar, K. R., De Leeuw, G., Lu, W., Huang, Q., & Zhu, X. X. (2020). Establishment of conceptual schemas of surface synoptic meteorological situations affecting fine particulate pollution across Eastern China in the winter. *Journal of Geophysical Research: Atmospheres*, *125*(23), e2020JD033153. https://doi.org/10.1029/2020JD033153

Huang, X., Ding, A. J., Wang, Z. L., Ding, K., Gao, J., Chai, F. H., & Fu, C. B. (2020). Amplified transboundary transport of haze by aerosol–boundary layer interaction in China. *Nature Geoscience*, *13*(6), 428–434. https://doi.org/10.1038/s41561-020-0583-4

Kang, H., Zhu, B., Gao, J., He, Y., Wang, H., Su, J., et al. (2019). Potential impacts of cold frontal passage on air quality over the Yangtze River Delta, China. *Atmospheric Chemistry and Physics*, *19*, 3673–3685. https://doi.org/10.5194/acp-19-3673-2019

Leung, D. M., Tai, A. P. K., Mickley, L. J., Moch, J. M., van Donkelaar, A., Shen, L., & Martin, R. V. (2018). Synoptic meteorological modes of variability for fine particulate matter ($PM_{2.5}$) air quality in major metropolitan regions of China. *Atmospheric Chemistry and Physics*, *18*(9), 6733–6748. https://doi.org/10.5194/acp-18-6733-2018

Li, J., Du, H. Y., Wang, Z. F., Sun, Y. L., Yang, W. Y., Li, J. Q., et al. (2017). Rapid formation of a severe regional winter haze episode over a mega-city cluster on the North China Plain. *Environmental Pollution*, *223*, 605–615. https://doi.org/10.1016/j.envpol.2017.01.063

Li, J. P., & Zeng, Q. C. (2002). A unified monsoon index. *Geophysical Research Letters*, *29*(8), 115-1–115-4. https://doi.org/10.1029/2001GL013874

Li, K., Jacob, D. J., Liao, H., Shen, L., Zhang, Q., & Bates, K. H. (2019). Anthropogenic drivers of 2013–2017 trends in summer surface ozone in China. *Proceedings of the National Academy of Sciences*, *116*(2), 422–427. https://doi.org/10.1073/pnas.1812168116

Li, Z. Q., Guo, J. P., Ding, A. J., Liao, H., Liu, J. J., Sun, Y. L., et al. (2017). Aerosol and boundary-layer interactions and impact on air quality. *National Science Review*, *4*(6), 810–833. https://doi.org/10.1093/nsr/nwx117

Liu, X. H., Zhu, B., Kang, H. Q., Hou, X. W., Gao, J. H., Kuang, X., et al. (2020). Stable and transport indices applied to winter air pollution over the Yangtze River Delta, China. *Environmental Pollution*, *227*, 115954. https://doi.org/10.1016/j.envpol.2020.115954

Lou, M. Y., Guo, J. P., Wang, L. L., Xu, H., Chen, D., Miao, Y., et al. (2019). On the relationship between aerosol and boundary layer height in summer in China under different thermodynamic conditions. *Earth and Space Science*, *6*(5), 887–901. https://doi.org/10.1029/2019EA000620

MEE (Ministry of Ecology and Environment of the People's Republic of China, the former Ministry of Environmental Protection). (2012). Ambient air quality standards, GB 3095-2012.

Otero, N., Sillmann, J., Mar, K. A., Rust, H. W., Solberg, S., Andersson, C., et al. (2018). A multi-model comparison of meteorological drivers of surface ozone over Europe. *Atmospheric Chemistry and Physics*, *18*(16), 12269–12288. https://doi.org/10.5194/acp-18-12269-2018

Shen, L., Mickley, L. J., & Murray, L. T. (2017). Influence of 2000–2050 climate change on particulate matter in the United States: Results from a new statistical model. *Atmospheric Chemistry and Physics*, *17*(6), 4355–4367. https://doi.org/10.5194/acp-17-4355-2017

Tai, A. P. K., Mickley, L. J., & Jacob, D. J. (2010). Correlations between fine particulate matter ($PM_{2.5}$) and meteorological variables in the United States: Implications for the sensitivity of $PM_{2.5}$ to climate change. *Atmospheric Environment*, *44*(32), 3976–3984. https://doi.org/10.1016/j.atmosenv.2010.06.060

Tie, X., Huang, R. J., Cao, J., Zhang, Q., Cheng, Y., Su, H., et al. (2017). Severe pollution in China amplified by atmospheric moisture. *Science Report*, *7*(1), 15760. https://doi.org/10.1038/s41598-017-15909-1

Wang, H. J., & Jiang, D. B. (2004). A new East Asian winter monsoon intensity index and atmospheric circulation comparison between strong and weak composite. *Quaternary Sciences (in Chinese)*, *24*(1), 19–27.

Wang, L., Chen, W., Zhou, W., & Huang, R. H. (2009). Interannual variations of East Asian trough axis at 500 hPa and its association with the East Asian winter monsoon pathway. *Journal of Climate*, *22*(3), 600–614. https://doi.org/10.1175/2008JCLI2295.1

Wang, Z. L., Huang, X., Ding, K., Ren, C. H., Cao, L., Zhou, D. R., et al. (2021). Weakened aerosol-PBL interaction during COVID-19 lockdown in Northern China. *Geophysical Research Letters*, *48*(3), e2020GL090542. https://doi.org/10.1029/2020GL090542

Xu, W. Y., Zhao, C. S., Ran, L., Deng, Z. Z., Liu, P. F., Na, N., et al. (2011). Characteristics of pollutants and their correlation to meteorological conditions at a suburban site in the North China Plain. *Atmospheric Chemistry and Physics*, *11*(9), 4353–4369. https://doi.org/10.5194/acp-11-4353-2011

Yang, W. Y., Du, H. Y., Wang, Z. F., Zhu, L. L., Wang, Z., Chen, X. S., et al. (2021). Characteristics of regional transport during two-year wintertime haze episodes in North China megacities. *Atmospheric Research*, *257*, 105582. https://doi.org/10.1016/j.atmosres.2021.105582

Zhai, S. X., Jacob, D. J., Wang, X., Shen, L., Li, K., Zhang, Y. Z., et al. (2019). Fine particulate matter ($PM_{2.5}$) trends in China, 2013-2018: Separating contributions from anthropogenic emissions and meteorology. *Atmospheric Chemistry and Physics*, *19*(16), 11031–11041. https://doi.org/10.5194/acp-19-11031-2019

Zhang, Q., Zheng, Y. X., Tong, D., Shao, M., Wang, S., Zhang, Y., et al. (2019). Drivers of improved $PM_{2.5}$ air quality in China from 2013 to 2017. *Proceedings of the National Academy of Sciences*, *116*(49), 24463–24469. https://doi.org/10.1073/pnas.1907956116

Zhang, W. C, Guo, J. P., Miao, Y. C., Liu, H., Song, Y., Fang, Z., et al. (2018). On the summertime planetary boundary layer with different thermodynamic stability in China: A radiosonde perspective. *Journal of Climate*, *31*(4), 1451–1465. https://doi.org/10.1175/JCLI-D-17-0231.1

Zhang, X. Y., Yin, Z. C., Wang, H. J., & Duan, M. K. (2021). Monthly variations of atmospheric circulations associated with haze pollution in the Yangtze River Delta and North China. *Advances in Atmospheric Sciences*, *38*, 569–580. https://doi.org/10.1007/s00376-020-0227-z

Zheng, B., Tong, D., Li, M., Liu, F., Hong, C., Geng, G., et al. (2018). Trends in China's anthropogenic emissions since 2010 as the consequence of clean air actions. *Atmospheric Chemistry and Physics*, *18*(19), 14095–14111. https://doi.org/10.5194/acp-18-14095-2018

References From the Supporting Information

Guo, J. P., Miao, Y. C., Zhang, Y., Liu, H., Li, Z. Q., Zhang, W. C., et al. (2016). The climatology of planetary boundary layer height in China derived from radiosonde and reanalysis data. *Atmospheric Chemistry and Physics*, *16*(20), 13309–13319. https://doi.org/10.5194/acp-16-13309-2016

Guo, J. P., Zhang, J., Yang, K., Liao, H., Zhang, S. D., Huang, K. M., et al. (2021). Investigation of near-global daytime boundary layer height using high-resolution radiosondes: First results and comparison with ERA5, MERRA-2, JRA-55, and NCEP-2 reanalyses. *Atmospheric Chemistry and Physics*, *21*(22), 17079–17097. https://doi.org/10.5194/acp-21-17079-2021

Seibert, P. F., Beyrich, P. F., Gryning, S. E., JoffreRasmussen, S. A., & Tercier, P. (2000). Review and intercomparison of operational methods for the determination of the mixing height. *Atmospheric Environment*, *34*(7), 1001–1027. https://doi.org/10.1016/S1352-2310(99)00349-0

Seidel, D. J., Ao, C. A., & Li, K. (2010). Estimating climatological planetary boundary layer heights from radiosonde observations: Comparison of methods and uncertainty analysis. *Journal of Geophysical Research*, *115*, D16113(D16), https://doi.org/10.1029/2009JD013680

Seidel, D. J., Zhang, Y. H., Beljaars, A., Golaz, J. C., Jacobson, A. R., & Medeiros, B. (2012). Climatology of the planetary boundary layer over the continental United States and Europe. *Journal of Geophysical Research*, *117*, D17106(D17), https://doi.org/10.1029/2012JD018143

Stull, R. B. (1988). *An introduction to boundary layer meteorology* (p. 666). Kluwer Academic

Vogelezang, D. H. P., & Holtslag, A. A. M. (1996). Evaluation and model impacts of alternative boundary-layer height formulations. *Boundary-Layer Meteorology*, *81*, 245–269. https://doi.org/10.1007/BF02430331

Von Engeln, A., & Teixeira, J. (2013). A planetary boundary layer height climatology derived from ECMWF reanalysis data. *Journal of Climate*, *26*(17), 6575–6590. https://doi.org/10.1175/JCLI-D-12-00385.1